



## Mapping Arctic Bottomfast Sea Ice Using SAR Interferometry

Downloaded from: <https://research.chalmers.se>, 2024-04-30 14:21 UTC


Citation for the original published paper (version of record):

Dammann, D., Eriksson, L., Mahoney, A. et al (2018). Mapping Arctic Bottomfast Sea Ice Using SAR Interferometry. Remote Sensing, 10(5). <http://dx.doi.org/10.3390/rs10050720>

N.B. When citing this work, cite the original published paper.

## Article

# Mapping Arctic Bottomfast Sea Ice Using SAR Interferometry

Dyre O. Dammann <sup>1,\*</sup> , Leif E. B. Eriksson <sup>1</sup>, Andrew R. Mahoney <sup>2</sup>, Christopher W. Stevens <sup>3</sup>, Joost van der Sanden <sup>4</sup>, Hajo Eicken <sup>5</sup>, Franz J. Meyer <sup>2</sup> and Craig E. Tweedie <sup>6</sup>

<sup>1</sup> Department of Space, Earth, and Environment, Chalmers University of Technology, Hörsalsvägen 11, 412 96 Gothenburg, Sweden; leif.eriksson@chalmers.se

<sup>2</sup> Geophysical Institute, University of Alaska Fairbanks, Fairbanks, Alaska, 2156 Koyukuk Drive, Fairbanks, AK 99775, USA; armahoney@alaska.edu (A.R.M.); fjmeyer@alaska.edu (F.J.M.)

<sup>3</sup> SRK Consulting (U.S.), Inc., 4700 Business Park Blvd, Anchorage, AK 99503, USA; cstevens@srk.com

<sup>4</sup> Canada Centre for Mapping and Earth Observation, 560 Rochester St., Ottawa, ON K1A 0E4, Canada; joost.vandersanden@canada.ca

<sup>5</sup> International Arctic Research Center, University of Alaska Fairbanks, Fairbanks, Alaska, 2160 Koyukuk Drive, Fairbanks, AK 99775, USA; heicken@alaska.edu

<sup>6</sup> Department of Biological Sciences, University of Texas El Paso, 500 W University Ave, El Paso, TX 79968, USA; ctweedie@utep.edu

\* Correspondence: dyre.dammann@chalmers.se; Tel.: +46-031-772-1577

Received: 6 April 2018; Accepted: 6 May 2018; Published: 7 May 2018



**Abstract:** Bottomfast sea ice is an integral part of many near-coastal Arctic ecosystems with implications for subsea permafrost, coastal stability and morphology. Bottomfast sea ice is also of great relevance to over-ice travel by coastal communities, industrial ice roads, and marine habitats. There are currently large uncertainties around where and how much bottomfast ice is present in the Arctic due to the lack of effective approaches for detecting bottomfast sea ice on large spatial scales. Here, we suggest a robust method capable of detecting bottomfast sea ice using spaceborne synthetic aperture radar interferometry. This approach is used to discriminate between slowly deforming floating ice and completely stationary bottomfast ice based on the interferometric phase. We validate the approach over freshwater ice in the Mackenzie Delta, Canada, and over sea ice in the Colville Delta and Elson Lagoon, Alaska. For these areas, bottomfast ice, as interpreted from the interferometric phase, shows high correlation with local bathymetry and in-situ ice auger and ground penetrating radar measurements. The technique is further used to track the seasonal evolution of bottomfast ice in the Kasegaluk Lagoon, Alaska, by identifying freeze-up progression and areas of liquid water throughout winter.

**Keywords:** sea ice; sea ice deformation; bottomfast ice; landfast sea ice; Arctic; synthetic aperture radar; InSAR

## 1. Introduction

### 1.1. Evolution and Relevance of Bottomfast Sea Ice

Arctic sea ice is a key component of the earth's climate system. It regulates absorbed solar radiation during summer and heat loss from the ocean in winter. The sea ice is also a critical component of coastal ecosystems, impacting Arctic flora, fauna, and coastal settlements. The landfast ice, a strip of ice anchored in place along the Arctic coastlines, is particularly significant and serves as an extension of the land for part of the year. It is used for denning by seals, migratory routes by caribou, and hunting of marine mammals by coastal populations [1]. In recent decades, Arctic sea ice has experienced

widespread retreat [2–4] including the landfast ice [5,6] leading to increased temperatures [7] and impacts on marine ecosystems [8] and coastal populations [9].

For the most part, the landfast sea ice is floating above the ocean floor, but in shallow areas such as in lagoons, near river deltas, and close to shore the ice can extend all the way to the seafloor under which condition it is known as bottomfast ice. During early fall freeze-up of Arctic coastlines, areas of bottomfast ice are narrow (Figure 1a), but can grow steadily over the winter months to the km-scale depending on the local bathymetry [10,11]. Such seasonal bottomfast sea ice allows for heat loss from the sea floor and is therefore an integral part of aggregating and maintaining subsea permafrost [11–13]. Bottomfast ice also controls coastal stability/morphology [14,15] and sediment properties that are particularly relevant to potential nearshore development of oil and gas resources [10]. In some areas, bottomfast ice freezes to the sea floor with a strength that inhibits vertical tidal lifts, resulting in an active tidal crack separating the bottomfast and floating parts of the landfast ice. Even so, the outer margins of the bottomfast ice can in some cases get torn loose from the sea floor during storm surges. The offshore progression of bottomfast ice commonly results in a series of inactive tidal cracks (Figure 1b).

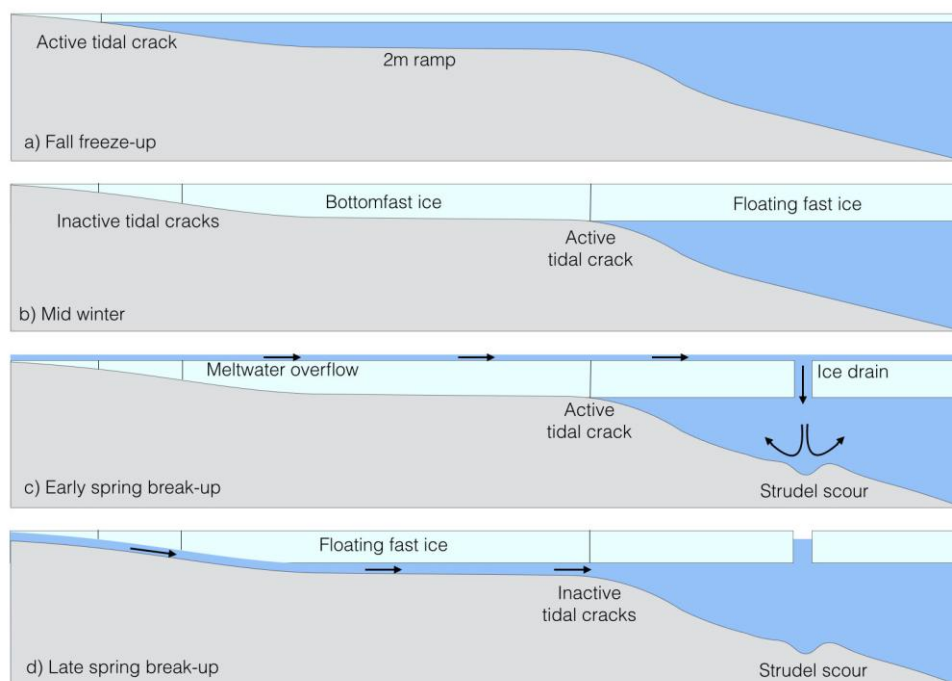


**Figure 1.** Schematic of seasonal evolution of bottomfast ice in a river delta where individual panels represent fall freeze-up (a), mid winter (b), early spring break-up (c), and late spring break-up (d).

During the early stage of spring melt in Arctic deltas, freshwater will flow on top of the bottomfast ice before reaching floating ice over deeper water. Here, the floating ice may break under the load of the overlaying water. The melt water will drain through cracks in the floating ice, which results in ice drains that can excavate deep into sea floor sediments (Figure 1c). The resulting indentations in the sea floor are known as strudel scours and occur mostly in the primary strudel zone, which is the area directly offshore of the bottomfast ice (an area between the 1.5 and 6 m isobaths) [16,17]. Strudel scour presents a major threat to subsurface infrastructure, particularly buried oil and gas pipelines [17], such as in the case of pipelines extending from the man-made Oooguruk Island near the Colville Delta [18]. In the event that a strudel drain is located directly above a buried subsea pipeline, a sufficiently deep strudel scour may expose the pipeline and lead to an unsupported span of pipeline. A strudel scour that forms directly over a buried pipeline also can remove the backfill material that is

needed to prevent damage from ice keels and forestall upheaval buckling [19]. Later in the spring the bottomfast ice will increasingly degrade as melt water starts to flow beneath the ice (Figure 1d) [20].

Bottomfast ice in Arctic lagoons plays an important role in controlling marine habitats by reducing areas that can be used for overwintering by fish in the same way as for lake ice [21]. Bottomfast ice is also significant for over-ice travel by coastal populations and for industrial ice operations by eliminating the risk of breaking through the ice. As an example, the construction of Oooguruk Island was dependent on bottomfast ice extending the entire way from the shore to the construction site [22]. However, the transition zone between bottomfast and floating ice is a high-risk zone for break-outs.

## 1.2. Remote Sensing of Bottomfast Sea Ice

Despite the widespread relevance of bottomfast sea ice to stakeholders and the scientific community, its areal extent in the Arctic is largely unknown with the exception of a few areas where in-situ measurements have been obtained. Poor bathymetric accuracy in many regions of the Arctic also makes it difficult to estimate which sections may be bottomfast. With rapid changes in ice thickness and the seasonal cycle of coastal sea ice [5], the extent and prevalence of bottomfast ice may have also changed substantially. However, there is insufficient data to evaluate such change. Remote sensing is the most opportune way to obtain cost-effective Arctic-wide coverage of bottomfast ice, but so far no consistent approach has been suggested. We show in this study that optical imagery may be able to aid in identification of bottomfast ice, but only during certain break-up conditions and at limited geographical locations.

Synthetic aperture radar (SAR) has shown utility for discriminating between floating and bottomfast ice in inland lakes [21]. For floating ice, the radar signal will reflect off the ice/water interface due to the high-contrast in dielectric properties between the two mediums. When ice becomes bottomfast, this dielectric high-contrast boundary disappears and most of the radar signal is absorbed in the sediments, leading to much lower backscatter [21,23,24]. For saline ice, the penetration of the SAR signal is reduced due to different salinity layers and brine inclusions, which results in a signal that may not reach the ice/water interface. For a SAR system with a relatively long wavelength such as PALSAR ( $\lambda \sim 23$  cm), the penetration may reach over 50 cm for ice colder than  $-5$  °C [25] for a typical ice salinity in the Beaufort Sea (5 ppt) [26]. In contrast, a system with shorter wavelength such as Sentinel-1 ( $\lambda \sim 5$  cm) the penetration is reduced to about 20 cm for the same salinity conditions [25]. Both SAR and polarimetric SAR (PolSAR) have produced good results in detecting bottomfast ice if there is sufficient penetration of the radar signal into the ice. Hence, detection of bottomfast ice in previous studies has focused on marine environments with almost no salinity such as the Mackenzie Delta [14,27]. Note that a SAR amplitude-based approach may be prone to generating false positives when the floating ice presents a backscatter signal similar as that of bottomfast ice, such as in cases where the floating ice is very smooth, which results in substantial specular reflection and low backscatter [27].

Synthetic aperture radar interferometry (InSAR) is sensitive to the motion of the landfast sea ice, which even in sheltered areas and in the absence of significant tidal amplitudes is typically on the order of cm/month for floating ice. This motion is largely due to thermal changes and can be detected with InSAR [28–30]. Bottomfast ice cannot move freely when undergoing thermal changes or propagating stress, and does not grow during the winter. Bottomfast ice is therefore found to retain interferometric coherence to a larger extent than floating ice, hence coherence can be used as an indication as to where the ice is bottomfast [27]. However, the floating fast ice also frequently retains high coherence. InSAR processing is also not only subject to temporal decorrelation due to ice motion, but also due to spatial, thermal noise, and process decorrelation [31,32]. Temporal decorrelation related to changes in dielectric constant or structure of the snow or ice is also relevant (e.g., due to melting/freezing events). Therefore, coherence can be reduced even in areas where the ice is bottomfast.

In this work, we apply the interferometric phase as a tool to detect bottomfast ice. Where the coherence is sufficient ( $>0.3$ ), the phase over sea ice is almost exclusively a result of vertical or horizontal motion [28], and hence can be used to detect areas of bottomfast ice where the ice is not free to move

and deform. We demonstrate the approach using the interferometric phase to delineate bottomfast ice for three different ice regimes (1) a freshwater delta; (2) a brackish delta; and (3) a saline lagoon. We validated InSAR-based bottomfast ice maps with a combination of in-situ measurements in areas of confirmed bottomfast ice (Mackenzie Delta, Canada) as well as with bathymetric information (Colville Delta and Elson Lagoon, Alaska). We also used the InSAR-based bottomfast ice mapping approach to analyze bottomfast ice formation in Kasegaluk Lagoon on a seasonal timescale.

## 2. Materials and Methods

### 2.1. Study Area

Three locations were used for a validation effort along the Beaufort Sea Coast: the Mackenzie and Colville deltas, as well as the Elson Lagoon (Figure 2). The Mackenzie Delta is one of the largest deltas in the Arctic and the surrounding waters and sea ice are almost completely fresh [12]. The near coastal ice used for validation in this area is first-year and predominately smooth ice. The shallow local bathymetry similar to other Arctic deltas [20] results in a girdle of bottomfast ice several kilometers wide.

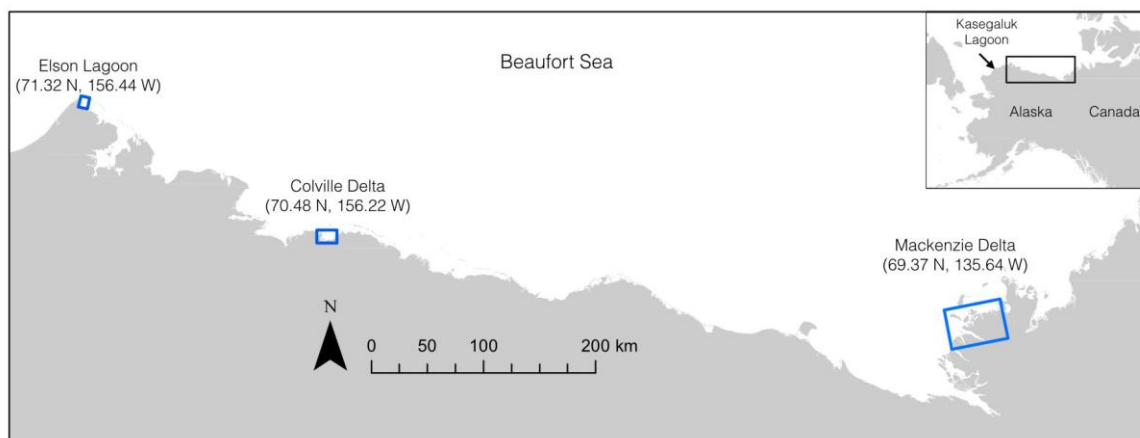


**Figure 2.** Overview map of three study areas on the Beaufort Sea coast.

The Colville Delta is the largest delta on the Alaska Arctic coast and is of major interest to oil and gas developers. The surrounding area features multiple drilling operations including the Oooguruk project. Sheltered by barrier islands in the eastern Harrison Bay, the sea ice consists of predominately smooth, first-year ice. In contrast to the Mackenzie Delta, the sea ice near the Colville Delta is saline due to a substantial decrease in water flow in winter [19]. According to USGS measurements at Umiat, Alaska, the November water flow is roughly 1% of that in the summer months and ceases almost completely by February. This leads to salt water penetration into the delta and water salinities close to those of ocean water [33]. The ice at Colville Delta is therefore expected to be brackish in the upper layer, but saline below.

Elson Lagoon is a semi-enclosed lagoon sheltered by barrier islands, which results in largely undeformed, level, first-year ice. The salinity of the sea ice is roughly that of ocean ice with mean values ranging between 4 ppt and 6 ppt in the central part of the ice column, based on ice cores obtained towards the end of the growth season [26].

### 2.2. Satellite Data

ALOS PALSAR L-band SAR data was used in the Mackenzie Delta (Section 3.1) due to its temporal overlap with in-situ data (Section 2.4). PALSAR, an L-band SAR system onboard the Japanese Advanced Land Observing Satellite (ALOS) operated between 2006 and 2011 with a repeat-pass time of 46 days. Sentinel-1 SAR data was used in the remaining two locations due to the free-and-open

nature of this data set and the regular coverage of recent acquisitions. Sentinel-1 is a constellation of two C-band sensors (Sentinel-1A and -1B) operating since 2014 and 2016 respectively, with a combined repeat-pass interval of 6 days. PALSAR and Sentinel-1 operate at different wavelengths and with different resulting penetration depth, but this is not critical for assessing sea ice deformation. Furthermore, there is no fundamental difference in the InSAR measurements provided by the two systems, hence, validation based on PALSAR is expected to hold across SAR systems, including Sentinel-1. Acquisition details for all interferograms can be found in Table 1.

**Table 1.** Image data for the interferograms used.

| Area           | Satellite  | Orbit        | Frame | Date                        | B <sub>T</sub> (d) | Θ         |
|----------------|------------|--------------|-------|-----------------------------|--------------------|-----------|
| Mackenzie      | PALSAR     | 05021, 05692 | 1390  | 3 January–18 February 2007  | 46                 | 36.6–40.9 |
| Mackenzie      | PALSAR     | 10389, 11060 | 1390  | 6 January–21 February 2008  | 45                 | 36.6–40.9 |
| Mackenzie      | PALSAR     | 15757, 16428 | 1390  | 8 January–23 February 2009  | 46                 | 36.6–40.9 |
| Mackenzie      | PALSAR     | 21125, 21796 | 1390  | 11 January–26 February 2010 | 45                 | 36.6–40.9 |
| Mackenzie      | PALSAR     | 21971, 22642 | 1390  | 10 March–25 April 2010      | 45                 | 36.6–40.9 |
| Colville Delta | Sentinel-1 | 5195, 5370   | 230   | 17–29 April 2017            | 12                 | 30.0–47.3 |
| Elson Lagoon   | Sentinel-1 | 5312, 5487   | 230   | 25 April–7 May 2017         | 12                 | 30.0–47.3 |
| Kasegaluk      | Sentinel-1 | 3708, 4058   | 226   | 5–29 January 2017           | 24                 | 30.0–47.4 |
| Kasegaluk      | Sentinel-1 | 4058, 4408   | 226   | 29 January–22 February 2017 | 24                 | 30.0–47.4 |
| Kasegaluk      | Sentinel-1 | 4408, 4583   | 226   | 22 February–6 March 2017    | 12                 | 30.0–47.4 |
| Kasegaluk      | Sentinel-1 | 4583, 4758   | 226   | 6–18 March 2017             | 12                 | 30.0–47.4 |
| Kasegaluk      | Sentinel-1 | 4758, 5108   | 226   | 18 March–11 April 2017      | 24                 | 30.0–47.4 |
| Kasegaluk      | Sentinel-1 | 5108, 5283   | 226   | 11–23 April 2017            | 12                 | 30.0–47.4 |
| Kasegaluk      | Sentinel-1 | 5283, 5633   | 226   | 23 April–17 May 2017        | 24                 | 30.0–47.4 |

All passes are ascending. B<sub>T</sub> = temporal baseline, d = days, Θ = incidence angle.

### 2.3. InSAR Processing and Concepts

InSAR is a technique that measures phase differences between two SAR scenes acquired from two similar viewing geometries [34,35]. Over sea ice, when a phase difference can be observed, it originates primarily from displacement of the scattering surface between acquisition pairs [28], represented by values between 0 and  $2\pi$  in the form of stripes (fringes) of equal phase change values. The phase values are sensitive to deformation in the order of millimeters. Therefore, InSAR can be used to detect small-scale displacements such as fractions of a full vertical tidal displacement and convergence as a result of temperature variations.

An interferogram can only be successfully created if the scattering properties of an analyzed surface remain largely unchanged. Coherence (ranging between 1 and 0) is a measure of the quality of the interferogram, which in general is high if scatterers remain unchanged and low if there is significant change in the scattering medium. For bottomfast ice, coherence is generally high enough to obtain an accurate phase value due to the high stability of the ice body in the absence of significant ice growth or deformation. However, during spring melt, the bottomfast ice is subject to substantial coherence loss due to wet snow on the ice, flooding, and detachment from the seafloor. It is therefore critical that SAR images used for bottomfast ice analysis are obtained prior to the onset of melt.

### 2.4. In-Situ Data for Validation

Bottomfast ice thickness surveys were obtained near Kendall Island in the Mackenzie Delta during March–April 2007 and April 2010 using auger measurements and ground penetrating radar (GPR) with an operating frequency of 500 MHz. A GPR system can be used to derive the thickness of floating ice from the return time of the radar signal reflecting back from the ice/water interface [36,37]. GPR systems can be used successfully on brackish ice near marine estuaries where the salinity is sufficiently low to allow for a signal return. This depends on radar frequency. Bottomfast ice can be determined using GPR due to the intermittent weakening or complete loss of signal return due to the absence of an ice/water interface [12,37,38]. The 2007 validation data collected was part of a two-season campaign



for winters 2005/2006 and 2006/2007. PALSAR data was not available for the first season, but in situ measurements provided insight as to bottomfast ice development and spatial distribution in the region [11]. The second season overlapped with PALSAR acquisitions and the GPR data could be directly applied for validation.

### 2.5. Freezing-Degree-Day Model to Estimate Ice Thickness

In the absence of direct ice thickness measurements, ice thickness ( $H$ ) can be estimated based on the air temperature during ice growth by using the freezing-degree-day model described by Anderson [39]:

$$H^2 + 5.1H = 6.7\theta \quad (1)$$

$$\theta = \int (T_w - T_a) dt \quad (2)$$

Freezing-degree-days,  $\theta$ , are calculated for discrete time steps of 1 day where  $T_a$  and  $T_w$  are the air and water temperature respectively. This approach has been shown to provide reasonable estimates of ice thickness compared to in-situ measurements [40].  $T_w$  is the water temperature at the ice/water interface and is equal to the freezing temperature of water.  $T_w$  depends on the water salinity and is  $-1.9$  and  $0$  °C for sea- and freshwater respectively.  $T_a$  and  $T_w$  are given in °C. The coefficients in Equation (1) assume a snow depth of 13% of the total ice thickness corresponding to a total of roughly 20 cm of snow. Furthermore, the ice draft (depth of the ice/water interface) can be calculated assuming hydrostatic equilibrium:

$$d = \frac{h_i \rho_i + h_s \rho_s}{\rho_w} \quad (3)$$

where  $d$  is the estimated draft and  $h_i$  and  $h_s$  are the ice thickness and snow depth respectively.  $\rho_i$ ,  $\rho_s$ , and  $\rho_w$  correspond to the density of ice ( $\sim 0.9$  kg dm $^{-3}$ ), snow ( $\sim 0.3$  kg dm $^{-3}$ ), and sea water ( $\sim 1$  kg dm $^{-3}$ ).

## 3. Results

We studied three locales along the Beaufort Sea coast (Figure 2) with the aim of validating the proposed approach and investigating potential applications for bottomfast ice mapping. These three study areas correspond to different ice regimes and provide an opportunity to explore different validation datasets and techniques. The proposed approach is first demonstrated in the Mackenzie Delta using in-situ ice auger and GPR measurements for validation (Section 3.1), then near the Colville Delta using bathymetry (Section 3.2), and finally in Elson Lagoon using Landsat 8 and high-resolution bathymetry data (Section 3.3).

### 3.1. Mackenzie Delta

The low bulk salinity of near-coastal ice at this site ensures strong radar return signals from the ice/water interface for floating ice. Hence, bottomfast ice can be identified as low-backscatter regions in PALSAR backscatter images with radar energy penetrating into the seafloor in the absence of an ice/water interface (Figure 3a). This was confirmed by auger measurements in two locations (red and yellow dots in Figure 3b,c). The exact location of the transition zone was obtained using GPR (orange). Compared with the interferograms (constructed between the prior images and the ones featured in Figure 3a,d), the areas featuring reduced backscatter appear with a consistent fringe signature similar to the signature over land (Figure 3d–f).

If there are no co-registration errors or atmospheric effects impacting the interferograms, the bottomfast ice will appear with a uniform phase value similar to level areas of land located near the shoreline. This is the case for the right interferogram shown in Figure 3d. The ice further offshore where there are no fringes is assumed to be floating. It has lost coherence as a result of either (1) lateral or vertical shifts due to internal stress or tidal motion; or (2) significant growth or melt at the ice/water

interface showing an altered backscatter surface (see white arrows for examples). The possibility that the ice could have been in a state of drift can be ruled out based on intermittent fringes and increased coherence further out (see red arrows). The left interferogram shown in Figure 3d features fringes extending across low-laying land (highlighted with a semi-transparent mask). The ice closest to shore also possesses the same large fringe spacing and is without discontinuities at the coastline. Hence, we can assume they are not attributed to ice motion and therefore the ice is likely bottomfast.

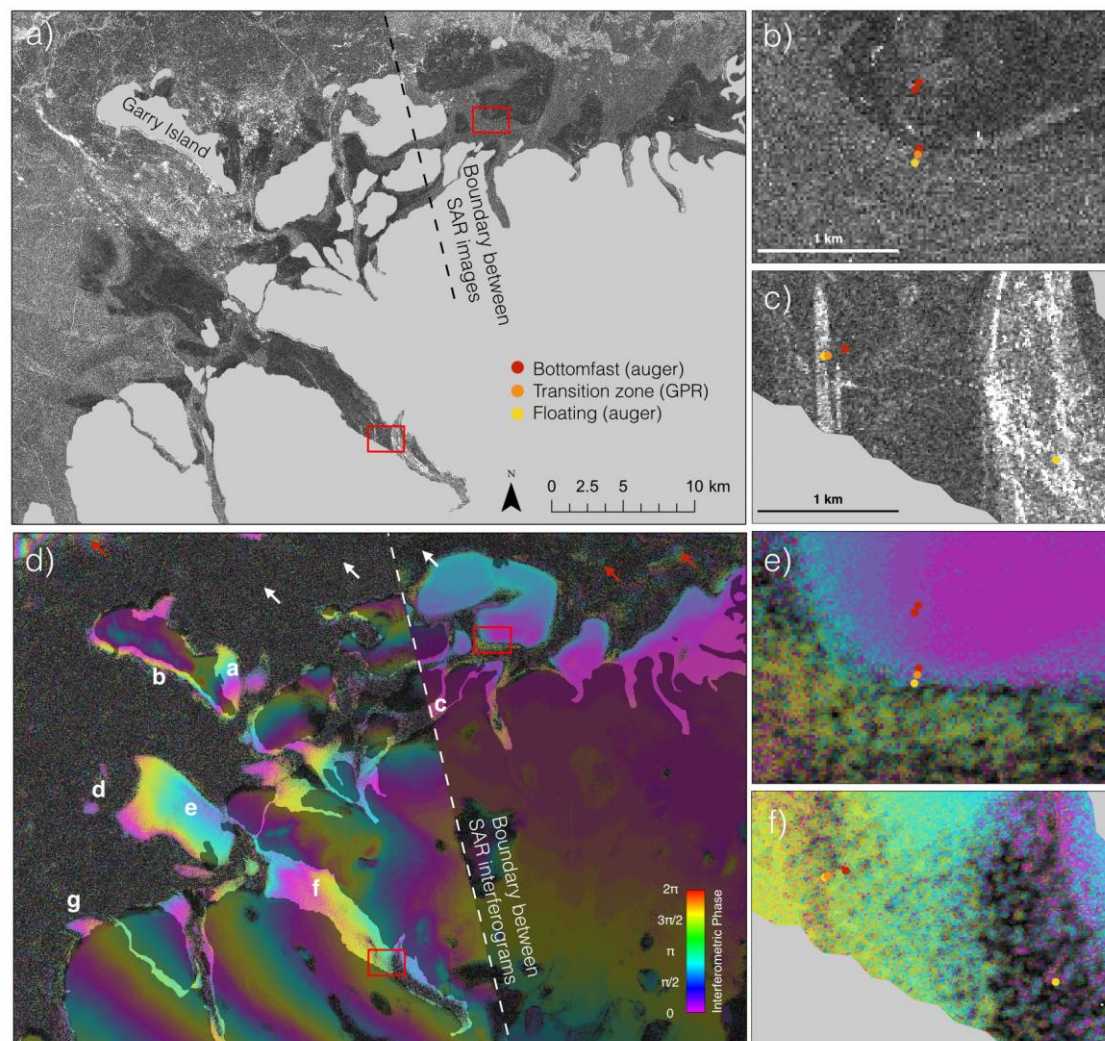


**Figure 3.** (a) Two PALSAR backscatter images acquired on 26 February 2010 (left) and 25 April 2010 (right) near Kendall Island, Mackenzie Delta; (b,c) Enlarged areas around in-situ measurements acquired on 25 April 2010 using auger and GPR; (d) Interferogram created using acquisitions from 10 March and 25 April 2010 (right) and 11 January and 26 February 2010 (left); (e,f) Enlarged areas around in-situ measurements.

Much of the ice that we assumed to be bottomfast in 2010 was confirmed bottomfast during two field campaigns in 2005/2006 and 2006/2007 (areas a–g in Figure 3d). We further compared a delineation of similar low-phase-ramp interferometric features early in 2007. We used a GPR track and auger measurements of bottomfast ice taken later the same year during the approximate maximum bottomfast ice extent (Figure 4). The in-situ measurements were collected at a later date than the acquisition of the PALSAR images, which results in a larger extent of bottomfast ice in the in-situ data. Even so, there is a clear correlation between the areas determined bottomfast in-situ (red) and using interferometric phase (light gray). Using interferograms from multiple years we tracked how the areas



occupied by bottomfast ice persist from year to year (colored lines in Figure 4). InSAR-compatible PALSAR scenes were only available prior to reaching maximum ice thickness, but they indicate reduced bottomfast ice extent during the in-situ campaigns (2007 and 2010) compared to 2008 and 2009.

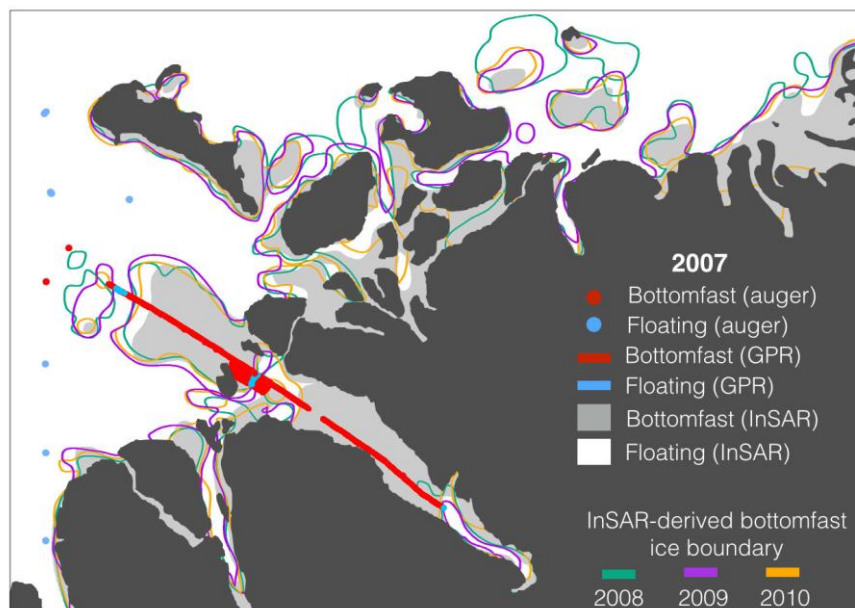


**Figure 4.** Bottomfast ice near Kendall Island, Mackenzie Delta, Canada spring 2007 delineated from an ALOS PALSAR interferogram from 3 January to 18 February (light gray). Auger validation points were acquired 19 March–2 April and GPR data on 28–29 March. In addition, InSAR-derived bottomfast ice is delineated for proceeding years using acquisitions from 6 January and 21 February 2008 (green), 8 January and 23 February 2009 (purple), and 11 January and 26 February 2010 (yellow).

### 3.2. Colville Delta

Oooguruk Island is connected to land by a seasonal ice road that is used for logistical transport and resupply during winter months and is a key part of its year-round operation. The island and ice road are visible in the Sentinel-1 backscatter image as a bright rectangular feature connected to land with a straight line. The surroundings feature a homogenous low backscatter area, corresponding to a uniform air/ice and/or ice/water interface (Figure 5a). In contrast to the Mackenzie Delta, no distinct stark gradients in backscatter indicative of bottomfast ice are apparent. A lack of such gradients is attributed to higher salinity and a shorter wavelength reducing penetration depth. In contrast to the Mackenzie River, the Colville River freezes before the formation of the landfast ice. This results in significantly reduced water flow leading to ice salinity that is close to that of offshore sea ice in the region [41]. If we superimpose the interferometric phase however (Figure 5b), two distinct areas separated by a high-contrasting phase boundary become apparent. One area features a phase similar to land and the near-shore areas of the delta (left side of the interferogram). To confirm that this abrupt change in interferometric phase is in fact the boundary between bottomfast and floating ice, we compared the phase with bathymetry data. Several bathymetry points were collected by Pioneer, the major operator of the Oooguruk project, during the summers of 2005 and 2006 [19] and provided by the US Bureau of Ocean and Energy Management (BOEM). Using a freezing-degree-day model (Equations (1) and (2)), we estimated the ice thickness to be between 1.37 m and 1.42 m (depending on freeze-up starting at the beginning of December or in the middle of October, respectively), assuming water salinity of sea water ( $-1.9\text{ }^{\circ}\text{C}$ ), and the surface air temperature to be equal to temperature recorded in Deadhorse, Alaska (roughly 70 km to the southeast of the Colville Delta).

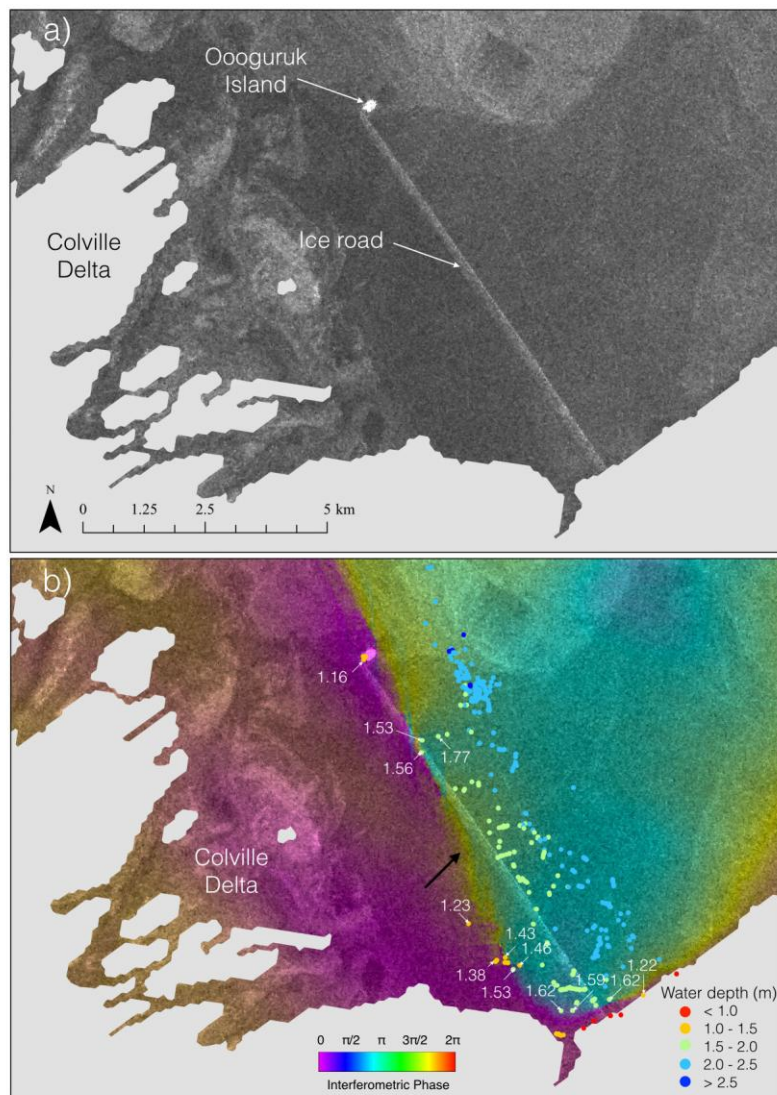


**Figure 5.** Sentinel-1 backscatter image over Colville River Delta 17 April 2017 (a) and superimposed interferometric phase values created using the following acquisition on 29 April 2017 (b). Bathymetric survey points based on survey data from 2005 to 2006. Estimated ice draft on 17 April based on surface air temperatures recorded in Deadhorse, Alaska, is  $\sim 1.35$  m.

The estimated ice thickness is associated with uncertainties since it depends on spatial and temporal factors that control ice growth, such as variation in salinity and snow depth. The water bathymetry may also have changed during the ten years between the bathymetry survey and the interferogram. Even so, it is a striking correlation between the bathymetry data, the estimated ice draft (1.35 m calculated from Equation (3)), and the high contrast phase boundary. The contrasting phase boundary correctly tracks isobaths ranging from 1.39 m to 1.42 m drawn up from the bathymetry points and lends further support to the interpretation that the phase boundary does in fact correspond to the sea ice grounding line. In a 1971 study of flooding of coastal ice, Walker [41] delineates the extent of surface ice flooding of the Colville River delta. His delineation of what we infer to be bottomfast ice, based on subsurface drainage and diversion of flood waters under floating ice, corresponds closely to the pattern shown in Figure 5b.

### 3.3. Elson Lagoon

The western Elson Lagoon features shallow near-coastal areas with bottomfast ice. Most noteworthy is a shoal extending northward from Tekegakkrok Point. A Sentinel-1 interferogram constructed over the area during spring 2017 is displayed in Figure 6a. Detailed bathymetry points were collected in Elson Lagoon in July 2015 with high-resolution DGPS and a single-beam sonar with 2.3 cm and 4.6 cm accuracy in the horizontal and vertical respectively and interpolated into a 10 m resolution surface [42] (Figure 6b). The interferogram displays constant phase values along the shallow western coastline as well as along the shoal consistent with the local bathymetry shown in Figure 6b.

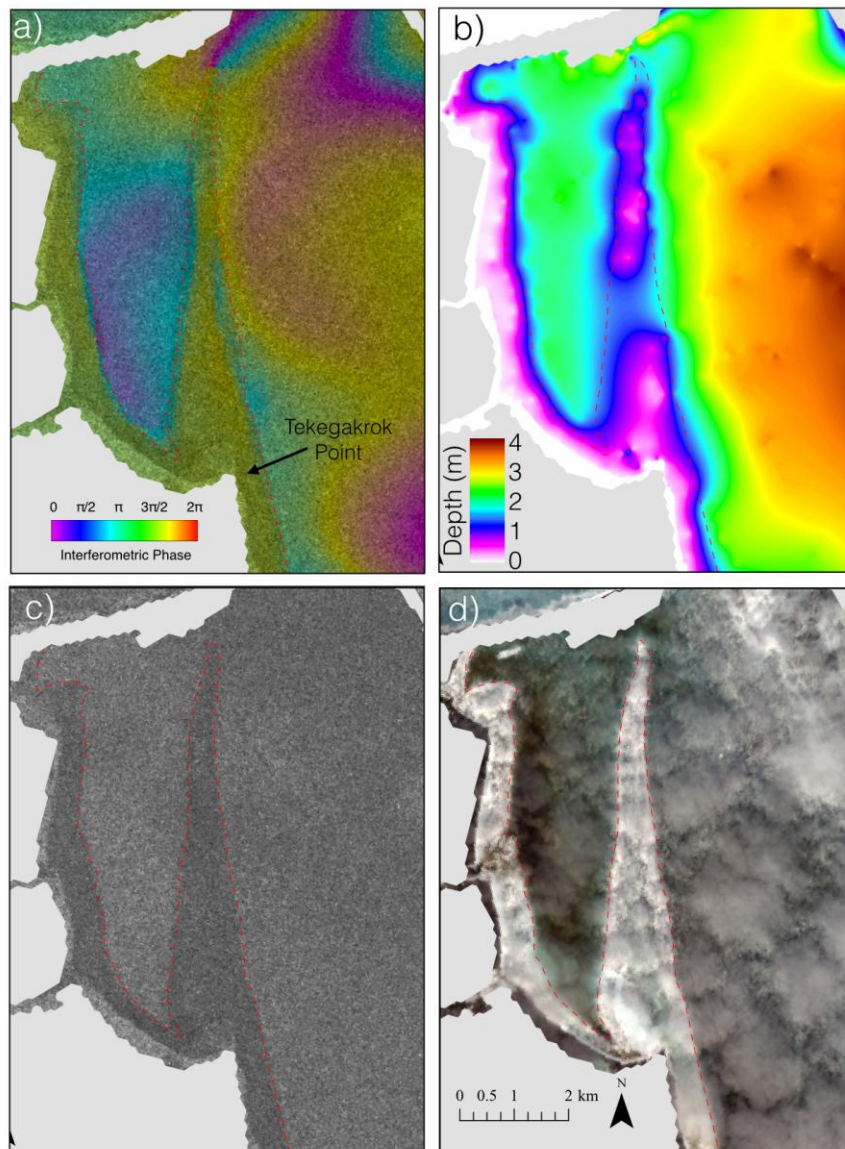


**Figure 6.** Western part of Elson Lagoon, near Point Barrow, Alaska. (a) Sentinel-1 interferogram between 25 April and 9 May 2017 superimposed on backscatter from 25 April 2017; (b) interpolated depth; (c) Sentinel-1 backscatter from 25 April 2017; and (d) Landsat 8 image from 27 May 2015. Dashed red line is based on outline of bottomfast ice as seen in (d). Land is masked out in light gray.

The master image of the interferogram displays largely homogenous backscatter across the lagoon largely due to the smooth ice conditions. However, the area of bottomfast ice is appearing with lower backscatter similar to the Mackenzie Delta, only less pronounced. This is surprising since the



water salinity in Elson Lagoon is close to that of sea water, hence the C-band signal penetration is not expected to be sufficient to reach the ice/water interface around the shoal. In previously analyzed C- and L-band imagery, the shoal has either not been detectable with SAR or has appeared with higher backscatter than the surrounding ice. This is likely attributed to either (1) earlier freeze-up with more vigorous frazil ice formation; or (2) formation of anchor ice over the shoal impacting surface roughness [43]. Although backscatter alone may be sufficient to delineate bottomfast ice here, it is not the case for most seasons.

Similar to SAR backscatter, optical imagery can give an indication of where the ice is bottomfast since bottomfast ice frequently features higher elevation than surrounding floating ice. During spring flooding, melt water will follow lower-laying floating ice, therefore it can be used to distinguish areas that are bottomfast. However, this only occurs under certain ice and flooding conditions discussed further in Section 4.3. The necessary conditions were not occurring in 2017 and we therefore drew upon a Landsat-8 image from break-up in 2015. Here, the “true-color” image (bands 2–4) displays lighter non-flooded areas (beneath a thin cloud layer), which match the areas of bottomfast ice (Figure 6d). A delineation of this area matches perfectly with the low-backscatter area (dashed line in Figure 6c). The average bathymetric depth along this line (1.28 m) comes to within 8 cm of the ice draft (1.20 m) calculated from average auger-confirmed ice thickness (1.24 m) and snow depth (0.24 m) collected in the western part of Elson Lagoon on 9 May 2017. The phase signature also corresponds well, with the exception of the central part of the shoal that features a narrower strip of consistent phase signature (Figure 6a). We speculate that the ice on each side of the shoal is resting on the sea floor, but not all is attached sufficiently to completely restrict tidal motion.

## 4. Discussion

### 4.1. Delineation Constraints

In Section 3, we demonstrated that the interferometric phase and, more specifically, phase values corresponding to those of adjacent low-laying land surfaces can be used as an indicator for bottomfast ice. Abrupt loss of coherence or phase gradients may furthermore pinpoint locations of tidal cracks and help delineate the exact location and extent of bottomfast sea ice. A good example of an abrupt change of phase can be seen in Figure 5b along most of the bottomfast ice. Here, bottomfast ice extent corresponds to the area enclosed between this phase discontinuity and the coastline. The coastline in this study has been obtained from the SAR imagery, which provides higher accuracy than the landmask [44], where coastline delineation can be off by up to 0.5 km (Figure 6a). However, there are also cases where the phase transitions smoothly from the bottomfast ice (see black arrow in Figure 5b). If the bottomfast ice grows substantially between acquisitions or the floating ice motion progresses smoothly from the undeformed bottomfast to the floating ice, it can be difficult to determine the exact location of the boundary. This can be the case if the relative displacement of the floating ice (due to atmosphere, ocean, or ice forcing) is small (sub mm-scale per day), which can result in less than one phase cycle (fringe) over distances approaching the km-scale. However, difficulty in determining the exact boundary can also occur with more substantial deformation if fringes extend parallel to the bottomfast ice, which is the case with shear motion along the coast, but does not occur if fringes are oriented at an angle. From SAR data alone, it can sometimes be difficult to determine which low-lying sediment bars in deltas are slightly below the surface and hence covered with a layer of ice and which ones are not. Here, additional datasets such as optical imagery are needed to accurately determine what is land.

With the use of InSAR, there are temporal restrictions both in terms of when suitable image pairs are available and during what time of the year they can be used. Here, an increasing number of operational and planned SAR systems (Sentinel-1, PALSAR-2, NISAR, Radarsat Constellation) will help reduce temporal restrictions. Interferograms quickly lose coherence upon the onset of melt; hence the last acquisition used in deriving an interferogram will have to be acquired prior to the beginning

of the melt season. These temporal restrictions impact the time frame over which bottomfast ice extent can be determined using InSAR. Typically, the last successful interferogram of the season is acquired one repeat cycle ahead of the date of attainment of maximum extent/thickness for the SAR system (6 days for Sentinel-1). With that said, even for systems with temporal baselines in the order of weeks, ice accretion towards the end of the ice growth season is expected to be minimal. Reduced growth is due to warmer temperatures and the relatively large ice thickness, leading to potentially minimal differences in bottomfast ice between March and May, as discussed below.

#### 4.2. Tracking Bottomfast Ice on a Seasonal Scale

Although delineation of the maximum extent of bottomfast ice can be useful, it can also be valuable to track the evolution of bottomfast ice within a season. This can especially be relevant for on-ice operations where it is necessary to determine exactly when the bottomfast ice forms (i.e., when the ice reaches maximum load bearing capacity). It is also a good measure of lagoon sub-ice aquatic habitat relevant to fish species and benthic organisms. As an example, we constructed seven Sentinel-1 interferograms over Kasegaluk Lagoon in Alaska, during winter and spring 2017 (Figure 7). The 120 km long lagoon is shallow, with an assumed maximum depth of about 4 m, but with most of the lagoon 1–2 m deep [45].

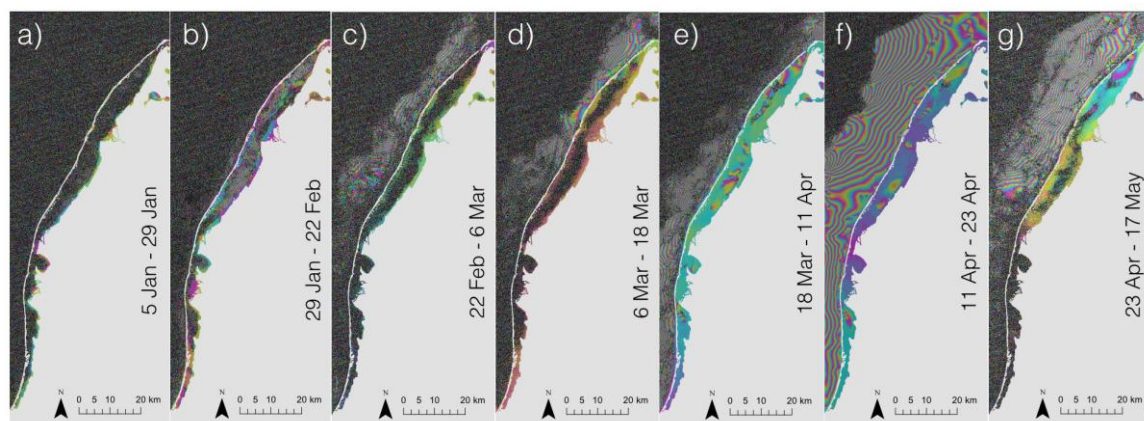


**Figure 7.** Bottomfast ice evolution in Kasegaluk Lagoon as interpreted through the phase signature of Sentinel-1 interferograms during winter and spring 2017. The individual panels represent time periods 5–29 January (a), 29 January–22 February (b), 22 February–6 March (c), 6–18 March (d), 18 March–11 April (e), 11–23 April (f), 23 April–17 May (g).

By the beginning of January (Figure 7a), there is generally only a narrow strip of bottomfast ice along the eastern shoreline. By the beginning of February (b), there is some bottomfast ice along both the eastern and western shorelines and a substantial part of the shallow southern part. Between late February and mid-March (c–d), the bottomfast ice expands to over halfway towards the center of the lagoon in several areas. Bottomfast ice covers most of the lagoon by mid-March (e), but only increases moderately in extent until early April (f). During late April and early May, the lagoon experiences melt processes leading to reduced coherence (g). This time series demonstrates that bottomfast ice extent can be tracked prior to melt and does not notably change between mid-March and the beginning of April (Figure 7e,f), indicating that extents derived as early as March are likely close to the seasonal maximum.

In this work, we are examining bottomfast ice formation in two lagoons that maintain large areas of liquid water during winter. These areas are of potential importance as a biological habitat and can possibly be used for overwintering by fish. Depending on location, the bottomfast ice can completely enclose pockets of liquid water. This is the case in Kasegaluk Lagoon and is known to occur in Elson Lagoon where the entire western part of the lagoon gets closed off by bottomfast ice along the shoal. During continued ice growth in winter, the salinity and pressure of the water underneath increases



steadily. In-situ measurements have confirmed excess pressure and water salinity values between 50 ppt and 70 ppt (unpublished data). In such cases it is critical to obtain quantitative data not just on where the bottomfast ice links up with the floating ice, but also about the changes in surface elevation in absolute terms of bottomfast ice and floating ice. InSAR can potentially help identify processes such as doming of floating ice due to excess water pressure or the interaction of bottomfast ice with subsea sediments as frozen sediments can lift up with the bottomfast ice. InSAR has a much larger potential than visible range imagery (Figure 6d) and SAR backscatter (Figure 6c) to fully understand these processes.

#### 4.3. Detection of Bottomfast Sea Ice Using Optical Imagery

Bottomfast ice has been found to have a higher elevation than the surrounding floating ice in the Colville Delta—likely attributed to tidal jacking (i.e., continued growth during high tides and storm surges). Under such conditions, 100% of bottom ice accretion will translate into increased elevation of the ice surface, while only 10% of bottom ice accretion under the floating ice contributes to increase in surface elevation [20]. Other possible contributing factors include (1) bottomfast ice will experience delayed bottom melt since warm water cannot access the ice bottom; or (2) bottomfast ice is colder at the end of winter than floating ice (since the bottom temperature is not constrained to the freezing point of seawater), prolonging the persistence of the ice cover prior to warming and complete melt; or (3) during periods of low sea level, the surrounding floating ice will drop, leaving bottomfast standing higher. In a case where the bottomfast ice is elevated compared to the floating ice, spring melt water may flood sections of the floating ice, but not the bottomfast ice. This was observed in Elson Lagoon during spring 2015 using Landsat 8 revealing an ice surface elevated above the darker flooded ice. This image allowed for a delineation of the bottomfast ice along a shoal sticking out in the western part of the lagoon (Figure 6d). However, interpretation of optical imagery should be used with caution due to the difficulty of interpreting bottomfast ice through clouds. Also, sediment-laden floodwater from land can potentially complicate interpretation during years where the shoal ice contains higher sediment concentrations than surrounding ice.

It is worth noting that in other areas, such as the Mackenzie Delta, the bottomfast ice surface is known to have a lower elevation than the surrounding ice and is more susceptible to spring flooding [11]. A possible explanation is shallower water leading to earlier formation of bottomfast ice and a shallower active layer of permafrost, which results in a strong bond with the frozen sediments preventing movement with tidal motion and tidal jacking. This will result in restricted ice growth and reduced elevation of the bottomfast ice surface in contrast to floating ice that further increases freeboard throughout winter. In such cases, flooding is largely restricted to the area of the bottomfast ice due to the active tidal crack separating floating and bottomfast ice where the floodwater can drain. Here, bottomfast ice controls spring overflow and potential strudel scours, constrains channel mouths, and affects early breakup season flood routing [27]. Regardless of the relative elevation of the bottomfast ice surface, delineation based on floodwater can only be done during flooding and is only possible during certain melt conditions, depending largely on the rate of melt.

## 5. Conclusions

This work presents an approach for consistently and rigorously determining the extent of bottomfast ice by identifying areas of near-zero phase values through spaceborne synthetic aperture radar interferometry (InSAR). The approach was successfully validated in fresh water near the Mackenzie Delta featuring low phase values and high coherence in areas of bottomfast ice confirmed using ground penetrating radar (GPR) and auger measurements. Similar results were obtained in saline ice near the Colville Delta where a strong phase gradient closely matched the approximate 1.4 m isobath. In Elson Lagoon, we found near-zero phase values consistent with local bathymetry as well as SAR backscatter and optical imagery. These results indicate that InSAR can consistently be used to map bottomfast sea ice in different regions and salinity regimes with both C- and L-band sensors.

InSAR was further used to map bottomfast ice evolution in Kasegaluk Lagoon, demonstrating the utility for consistently mapping bottomfast ice on seasonal timescales before the onset of melt. This creates opportunities to determine long-term changes in the extent of bottomfast sea ice over large swaths of the Arctic on decadal timescales and using multiple platforms. Such studies are urgently needed because of the importance of bottomfast ice in constraining the location of permafrost-rich shorelines. There is currently uncertainty around the distribution of bottomfast ice and this can be addressed with the approach outlined here. More accurate estimates of the total extent of bottomfast ice would be relevant in terms of tracking and understanding large-scale changes, in particular in the scope of Arctic warming and the resulting degradation of subsea permafrost. Local data on bottomfast ice extent, seasonality, and long-term changes in key strategic areas would also be of relevance for ice use by coastal communities and for resource development.

In many nearshore areas, detailed bathymetric information is not readily accessible. Here, detailed information of the location of bottomfast ice could be relevant in determining the slope and small-scale topography of the <2 m deep inshore zone and the topographic bench in front of Arctic river deltas [15]. Combining a freezing-degree-day or full-scale ice growth model with InSAR data analysis could potentially be used to determine incremental bathymetric contours at locations of bottomfast ice based on sequences of interferograms during a season. Such maps could prove useful for near-shore navigation with smaller vessels and routing of subsurface pipelines that need to be protected from deep-draft ice keels. This technique could also potentially be used to track shallow-water bathymetric changes over time.

The bottomfast sea ice may be critical in terms of brine injection into the sediments and in its ability to conduct heat from frozen sediments to the atmosphere aiding in maintaining and aggregating subsea permafrost. The bottomfast ice delineation such as presented here is thus relevant in terms of coastal erosion by potentially providing insight and highlighting areas of unconsolidated, ice-bonded nearshore sediments where the bottomfast ice is essential in pinning the coastline [46]. Detailed information on locations of bottomfast ice will also have implications for landfast sea ice models. With the exception of grounded ridges, landfast sea ice is held in place by freezing into embayments or around islands. However, if an embayment freezes to the bottom, an oceanward tidal crack will form and may reduce or eliminate the stabilizing effect.

**Author Contributions:** D.O.D. conducted the interferometric processing and analysis and drafted the initial manuscript. L.E.B.E. and A.R.M. provided critical guidance on all aspects of the analysis and manuscript. C.W.S. and J.v.d.S. conducted the ground validation in July 2005 and 2010 respectively and provided valuable contributions from their knowledge of the Mackenzie Delta. H.E. and F.J.M. provided critical guidance drawing upon their expertise within sea ice and interferometric processing respectively. C.E.T. created the bathymetric dataset used for Elson Lagoon. All co-authors also provided valuable recommendations and corrections resulting in the final manuscript.

**Acknowledgments:** This work was funded in part by the Swedish National Space Board (Dnr 192/15), the Seasonal Ice Zone Observing Network (NSF-0856867), the Barrow Area Information Database (NSF-1023654), and the US Bureau of Ocean and Energy Management (BOEM) Coastal Impact Assistance Program. We acknowledge Alaska Satellite Facility for access to ALOS and Sentinel-1 data and, in particular, Bill Hauer for additional expertise and guidance. We acknowledge BOEM for access to bathymetry data. We thank Marguerite Tibbles and Dustin Whalen for providing guidance and knowledge gained from extensive field experience around their respective study areas. We thank Christopher Polashenski for providing ice thickness measurements and Guido Grosse for providing expertise related to subsea permafrost. We acknowledge Gaby Tarin for bathymetric data collection and Stephen Escarzaga and Ryan Cody for data processing and generation of bathymetric maps for Elson Lagoon.

**Conflicts of Interest:** The authors declare no conflict of interest.

## References

1. Eicken, H.; Lovcraft, A.L.; Druckenmiller, M.L. Sea-ice system services: A framework to help identify and meet information needs relevant for Arctic observing networks. *Arctic* **2009**, *62*, 119–136. [[CrossRef](#)]
2. Stroeve, J.C.; Serreze, M.C.; Holland, M.M.; Kay, J.E.; Malanik, J.; Barrett, A.P. The Arctic's rapidly shrinking sea ice cover: A research synthesis. *Clim. Chang.* **2012**, *110*, 1005–1027. [[CrossRef](#)]

3. Comiso, J.C.; Hall, D.K. Climate trends in the Arctic as observed from space. *Wiley Interdiscip. Rev. Clim. Chang.* **2014**, *5*, 389–409. [[CrossRef](#)] [[PubMed](#)]
4. Meier, W.N.; Hovelsrud, G.K.; Oort, B.E.; Key, J.R.; Kovacs, K.M.; Michel, C.; Haas, C.; Granskog, M.A.; Gerland, S.; Perovich, D.K. Arctic sea ice in transformation: A review of recent observed changes and impacts on biology and human activity. *Rev. Geophys.* **2014**, *52*, 185–217. [[CrossRef](#)]
5. Mahoney, A.; Eicken, H.; Gaylord, A.G.; Gens, R. Landfast sea ice extent in the Chukchi and Beaufort Seas: The annual cycle and decadal variability. *Cold Reg. Sci. Technol.* **2014**, *103*, 41–56. [[CrossRef](#)]
6. Selyuzhenok, V.; Krumpen, T.; Mahoney, A.; Janout, M.; Gerdes, R. Seasonal and interannual variability of fast ice extent in the southeastern Laptev Sea between 1999 and 2013. *J. Geophys. Res. Oceans* **2015**, *120*, 7791–7806. [[CrossRef](#)]
7. Screen, J.A.; Simmonds, I. The central role of diminishing sea ice in recent Arctic temperature amplification. *Nature* **2010**, *464*, 1334–1337. [[CrossRef](#)] [[PubMed](#)]
8. Post, E.; Bhatt, U.S.; Bitz, C.M.; Brodie, J.F.; Fulton, T.L.; Hebblewhite, M.; Kerby, J.; Kutz, S.J.; Stirling, I.; Walker, D.A. Ecological consequences of sea-ice decline. *Science* **2013**, *341*, 519–524. [[CrossRef](#)] [[PubMed](#)]
9. Dammann, D.O. Arctic Sea Ice Trafficability—New Strategies for a Changing Icescape. Ph.D. Thesis, University of Alaska Fairbanks, Fairbanks, AK, USA, 2017.
10. Solomon, S.M.; Taylor, A.E.; Stevens, C.W. Nearshore ground temperatures, seasonal ice bonding, and permafrost formation within the bottom-fast ice zone, Mackenzie Delta, NWT. In Proceedings of the Ninth International Conference on Permafrost, Fairbanks, AK, USA, 29 June–3 July 2008; University of Alaska Fairbanks: Fairbanks, AK, USA, 2008; pp. 1675–1680.
11. Stevens, C.W.; Moorman, B.J.; Solomon, S.M. Interannual changes in seasonal ground freezing and near-surface heat flow beneath bottom-fast ice in the near-shore zone, Mackenzie Delta, NWT, Canada. *Permafr. Periglac. Process.* **2010**, *21*, 256–270. [[CrossRef](#)]
12. Stevens, C.W.; Moorman, B.J.; Solomon, S.M. Detection of frozen and unfrozen interfaces with ground penetrating radar in the nearshore zone of the Mackenzie Delta, Canada. In Proceedings of the Ninth International Conference on Permafrost, Fairbanks, AK, USA, 29 June–3 July 2008; University of Alaska Fairbanks: Fairbanks, AK, USA, 2008; pp. 1711–1716.
13. Stevens, C.W. Controls on Seasonal Ground Freezing and Permafrost in the Near-Shore Zone of the Mackenzie Delta, NWT, Canada. Ph.D. Thesis, University of Calgary, Calgary, AB, Canada, 2011.
14. Eicken, H.; Dmitrenko, I.; Tyshko, K.; Darovskikh, A.; Dierking, W.; Blahak, U.; Groves, J.; Kassens, H. Zonation of the Laptev Sea landfast ice cover and its importance in a frozen estuary. *Glob. Planet. Chang.* **2005**, *48*, 55–83. [[CrossRef](#)]
15. Are, F.; Reimnitz, E. An overview of the Lena River Delta setting: Geology, tectonics, geomorphology, and hydrology. *J. Coast. Res.* **2000**, 1083–1093.
16. Leidersdorf, C.B.; Hearon, G.E.; Vaudrey, K.D.; Swank, G. Strudel scour formation off Arctic river deltas. In *Coastal Engineering 2006: (In 5 Volumes)*; World Scientific: Singapore, 2007; p. 5312.
17. Dickins, D.; Hearon, G.; Morris, K.; Ambrosius, K.; Horowitz, W. Mapping sea ice overflow using remote sensing: Alaskan Beaufort Sea. *Cold Reg. Sci. Technol.* **2011**, *65*, 275–285. [[CrossRef](#)]
18. Lanan, G.A.; Cowin, T.; Hazen, B.; Maguire, D.H.; Hall, J.D.; Perry, C.J. Oooguruk offshore Arctic flowline design and construction. In Proceedings of the Offshore Technology Conference, Houston, TX, USA, 5–8 May 2008.
19. Hearon, G.; Dickins, D.; Ambrosius, K.K.M. *Mapping Sea Ice Overflow Using Remote Sensing: Smith Bay to Camden Bay*; Report Prepared by DF Dickins Associates, Minerals Management Service, Alaska OCS Region under Contract M06PC00034; Coastal Frontiers Corporation, Aerometric, and The Geophysical Institute; University of Alaska for US Department of Interior: Fairbanks, AK, USA, 2009.
20. Reimnitz, E. Interaction of river discharge with sea ice in proximity of Arctic deltas: A review. *Polarforschung* **2002**, *70*, 123–134.
21. Hirose, T.; Kapfer, M.; Bennett, J.; Cott, P.; Manson, G.; Solomon, S. Bottomfast ice mapping and the measurement of ice thickness on tundra lakes using c-band synthetic aperture radar remote sensing. *J. Am. Water Resour. Assoc.* **2008**, *44*, 285–292. [[CrossRef](#)]
22. Hall, J. Oooguruk project offshore Alaska. *Offshore Magazine*, 1 August 2008; p. 68.

23. Engram, M.; Arp, C.D.; Jones, B.M.; Ajadi, O.A.; Meyer, F.J. Analyzing floating and bedfast lake ice regimes across Arctic Alaska using 25 years of space-borne SAR imagery. *Remote Sens. Environ.* **2018**, *209*, 660–676. [[CrossRef](#)]
24. Jeffries, M.; Morris, K.; Weeks, W.; Wakabayashi, H. Structural and stratigraphic features and ERS 1 synthetic aperture radar backscatter characteristics of ice growing on shallow lakes in NW Alaska, winter 1991–1992. *J. Geophys. Res. Oceans* **1994**, *99*, 22459–22471. [[CrossRef](#)]
25. Hallikainen, M.; Winebrenner, D.P. The physical basis for sea ice remote sensing. *Microw. Remote Sens. Sea Ice* **1992**, 29–46.
26. Oggier, M.; Eicken, H. Tabulation of first-year sea-ice properties representative of the annual cycle as relevant to 2014 oil-in-ice experiments project. In *Detection of Oil on-in-and-under Ice—Final Report 5.3*; Pegau, W.S., Garron, J., Zabilansky, L., Eds.; Arctic Response Technology: London, UK, 2016; pp. 251–264.
27. Yue, B.; Chamberland, J.; Mulvie, J. Bottom-fast ice delineation with polsar and insar techniques in the Mackenzie Delta Region, Northwest Territories, Canada. *Can. J. Remote Sens.* **2013**, *39*, 341–353. [[CrossRef](#)]
28. Dammann, D.O.; Eicken, H.; Meyer, F.; Mahoney, A. Assessing small-scale deformation and stability of landfast sea ice on seasonal timescales through l-band SAR interferometry and inverse modeling. *Remote Sens. Environ.* **2016**, *187*, 492–504. [[CrossRef](#)]
29. Berg, A.; Dammert, P.; Eriksson, L.E. X-band interferometric SAR observations of Baltic fast ice. *IEEE Trans. Geosci. Remote Sens.* **2015**, *53*, 1248–1256. [[CrossRef](#)]
30. Li, S.; Shapiro, L.; McNutt, L.; Feffers, A. Application of satellite radar interferometry to the detection of sea ice deformation. *J. Remote Sens. Soc. Jpn.* **1996**, *16*, 67–77.
31. Meyer, F.J.; Mahoney, A.R.; Eicken, H.; Denny, C.L.; Druckenmiller, H.C.; Hendricks, S. Mapping Arctic landfast ice extent using l-band synthetic aperture radar interferometry. *Remote Sens. Environ.* **2011**, *115*, 3029–3043. [[CrossRef](#)]
32. Zebker, H.A.; Villasenor, J. Decorrelation in interferometric radar echoes. *IEEE Trans. Geosci. Remote Sens.* **1992**, *30*, 950–959. [[CrossRef](#)]
33. Mikhailova, M. Hydrological processes at an Arctic river mouth: Case study of the Colville River, Alaska, USA. *Water Resour.* **2009**, *36*, 26–42. [[CrossRef](#)]
34. Ferretti, A.; Monti-Guarnieri, A.; Prati, C.; Rocca, F.; Massonet, D. Insar principles-guidelines for SAR interferometry processing and interpretation. *ESA Publ.* **2007**, TM-19, 40.
35. Bamler, R.; Hartl, P. Synthetic aperture radar interferometry. *Inverse Probl.* **1998**, *14*, R1. [[CrossRef](#)]
36. Haas, C.; Druckenmiller, M. Ice thickness and roughness measurements. In *Field Techniques for Sea Ice Research*; Eicken, H., Grading, R., Salganek, M., Shirasawa, K., Perovich, D., Leppäranta, M., Eds.; University of Alaska Press: Fairbanks, AK, USA, 2009; pp. 49–116.
37. Stevens, C.W.; Moorman, B.J.; Solomon, S.M.; Hugenholtz, C.H. Mapping subsurface conditions within the near-shore zone of an Arctic delta using ground penetrating radar. *Cold. Reg. Sci. Technol.* **2009**, *56*, 30–38. [[CrossRef](#)]
38. Dammann, D.O.; Eicken, H.; Mahoney, A.; Meyer, F.; Betcher, S. Assessing sea ice trafficability in a changing Arctic. *Arctic* **2018**, *71*, 59–75. [[CrossRef](#)]
39. Anderson, D.L. Growth rate of sea ice. *J. Glaciol.* **1961**, *3*, 1170–1172. [[CrossRef](#)]
40. Petrich, C.; Eicken, H. Growth, structure and properties of sea ice. In *Sea Ice*; Thomas, D.N., Dieckmann, G.S., Eds.; Wiley-Blackwell: Oxford, UK, 2010; Volume 2, pp. 23–77.
41. Walker, H. Spring discharge of an Arctic river determined from salinity measurements beneath sea ice. *Water Resour. Res.* **1973**, *9*, 474–480. [[CrossRef](#)]
42. Tweedie, C.E.; Escarzaga, S.; Manley, W.F.; Tarin, G.; Gaylord, A. Interpolated Bathymetric Surface for the Elson Lagoon, Barrow, Northern Alaska, 2015. Barrow Area Information Database (BAID), 2016. Digital Media. Available online: <http://barrowmapped.org> (accessed on 7 May 2018).
43. Stierle, A.P.; Eicken, H. Sediment inclusions in Alaskan coastal sea ice: Spatial distribution, interannual variability, and entrainment requirements. *Arct. Antarct. Alp. Res.* **2002**, *34*, 465–476. [[CrossRef](#)]
44. Wessel, P.; Smith, W.H. A global, self-consistent, hierarchical, high-resolution shoreline database. *J. Geophys. Res. Solid Earth* **1996**, *101*, 8741–8743. [[CrossRef](#)]

45. Frost, K.; Lowry, L.; Carroll, G. *Use of Kasegaluk Lagoon, Chukchi Sea, Alaska, by Marine Birds and Mammals, III: Marine Mammals*; Minerals Management Service, U.S. Department of Interior Anchorage, Alaska: Anchorage, AK, USA, 1992; p. 627.
46. Overduin, P.P.; Westermann, S.; Yoshikawa, K.; Haberlau, T.; Romanovsky, V.; Wetterich, S. Geoelectric observations of the degradation of nearshore submarine permafrost at Barrow (Alaskan Beaufort Sea). *J. Geophys. Res. Earth Surf.* **2012**, *117*. [[CrossRef](#)]



© 2018 by the authors. Licensee MDPI, Basel, Switzerland. This article is an open access article distributed under the terms and conditions of the Creative Commons Attribution (CC BY) license (<http://creativecommons.org/licenses/by/4.0/>).